Compact Long-Range Single-Photon Underwater Lidar With High Spatial–Temporal Resolution

Mingjia Shangguan, Zhifeng Yang, Zaifa Lin, Zhongping Lee, *Member, IEEE*, Haiyun Xia, and Zhenwu Weng

***Abstract*— Oceanic lidar has emerged as a strong technology for oceanic 3-D remote sensing. However, most existing oceanic lidars are bulky and high-power consumption and thus difficult to enable underwater operation. Here, we present a compact single-photon lidar system for long-range underwater measurement. A single-photon detector was adopted to achieve a high signal-to-noise ratio. Benefiting from the single-photon sensitivity in detection, long-range active detection was realized with a low pulse energy laser at 1 μJ and a small-aperture coupler at 12 mm. Moreover, a narrow linewidth picosecond fiber laser with high repetition rate was employed to guarantee a high spatial resolution and high update rate. A fiber-connected configuration was specially designed for the miniaturized and robust structure in an optical receiver. In an experimental demonstration, the profile of backscattered signal from clean water was obtained over 70 m with high spatial–temporal resolution to demonstrate the capability of this lidar system. The maximum detection distance of the single-photon lidar reaches $\sim 3.6/K_d$ (K_d is the diffuse attenuation coefficient) for waterbody and up to $5.5/K_d$ for a hard target. Furthermore, it exhibits a high update-rate capability and realizes the localization and quantification of underwater bubbles up to 26 m away at a high update rate of 100 Hz. These results indicate its potential in a variety of applications, including remote sensing of marine biogeochemical parameters, the quantification of seabed gas emissions, and long-range underwater imaging.**

***Index Terms*— Single-photon detector, underwater lidar.**

I. Introduction

SINCE lidar can operate at night, at high latitudes when solar radiation is low, and potentially penetrate the subsurface chlorophyll maximum zone, it has become the most important technology to supplement passive ocean-color remote sensing, which has provided a sustained synoptic view of the distribution of ocean's optical properties and biogeochemical parameters for the past 20-plus years [1], [2]. By extracting depolarization, Brillouin, Raman, and fluorescence information from the backscattered signal, oceanic lidar can retrieve a range of parameters, including phytoplankton [3], temperature [4], [5], bubbles [6], the dynamics of the upper ocean [7], and others [8]. To enhance detection capabilities, oceanic lidars have been deployed at different platforms, including underwater platforms autonomous inspection using an underwater 3-D lidar [9], surface vessels [10], aircraft [11], and satellites [12], [13]. To fit on small platforms, especially unmanned aerial vehicles (UAVs), some compact UAV-borne lidars have been developed for bathymetry measurement, including the RIEGL VQ-840-G [14], the ASTRALiTe edge[1] [15], and Fugro RAMMS [16]. However, most existing oceanic lidars for optical parameter detection of water are bulky and high in power consumption. Although tremendous efforts have been devoted to the development of a compact oceanographic lidar for long-range active detection with high depth-temporal resolution, but it is still a challenging task.

On the one hand, researchers have developed several oceanic lidars with high pulse energy to penetrate deeper into the ocean [17]. For instance, an oceanic lidar developed by the National Oceanic and Atmospheric Administration (NOAA) with pulse energy reaches 100 mJ at 532 nm has revealed the thin scattering layers below 40 m in oceanic waters [7]. On the other hand, oceanic lidar based on blue light has been proposed since blue laser has a much better penetration depth in the open ocean than green laser. An airborne dual-wavelength oceanic lidar has demonstrated that the vertical profiles obtained by the 486-nm laser can penetrate approximately 100 m in the South China Sea, which is ~25% more than that of a 532-nm laser [18].

However, increasing the pulse energy of the laser to achieve deeper penetration has several significant drawbacks. First, underwater plankton are subject to damage from high-energy laser, especially when the laser energy density is high in water, such as the application of shipborne or underwater lidar. Second, eye safety is also a crucial factor that must be considered. Furthermore, high power consumption limits its operation on some important platforms, such as UAVs or autonomous underwater vehicles (AUVs). In addition, although blue laser can improve the detection performance of lidar, the requirements of high pulse energy and its more complex structures limit its further application [19]. In view

Manuscript received 16 January 2023; revised 11 April 2023; accepted 4 May 2023. Date of publication 9 May 2023; date of current version 30 May 2023. This work was supported in part by the Natural Science Foundation of Fujian Province of China under Grant 2020J01026, in part by the Joint Funds of the National Natural Science Foundation of China under Grant U2106210, in part by the National Key Research and Development Program of China under Grant 2022YFB3901704, in part by the State Key Laboratory of Marine Environmental Science (MEL)-State Key Laboratory of Robotics (RLAB) Joint Fund for Marine Science and Technology Innovation, and in part by the MEL Internal Research Program under Grant MELRI2101. *(Corresponding author: Mingjia Shangguan.)*

Mingjia Shangguan, Zhifeng Yang, Zaifa Lin, Zhongping Lee, and Zhenwu Weng are with the State Key Laboratory of Marine Environmental Science and the Department of Applied Marine Physics and Engineering, College of Ocean and Earth Sciences, Xiamen University, Xiamen 361102, China (e-mail: mingjia@xmu.edu.cn).

Haiyun Xia is with the School of Atmospheric Physics, Nanjing University of Information Science and Technology, Nanjing 210044, China.

Digital Object Identifier 10.1109/LGRS.2023.3274449

[1]Trademarked.

of that current oceanic lidars are being high power consumption and bulky, a compact and low-power lidar system that can provide high spatial–temporal resolution profiles over long range with commercially available green laser is highly valuable, but not available yet. Fortunately, single-photon lidar has emerged as a strong candidate technology due to its high sensitivity. This technology has already been used in topographic and bathymetric mapping [12], [20], as well as atmospheric detection [21], [22]. However, to the best of our knowledge, there has been no reported application of single-photon-based underwater lidar for detecting water optical parameters. Since the penetration depth of laser in water is limited, an underwater lidar would greatly extend its performance, especially with the help of underwater platforms such as AUVs. In addition, interferences from the sea–air interface and atmospheric backscattered signal can be avoided, which is a great challenge for oceanic lidars that operate above the water [23].

II. Single-Photon Lidar System

In this letter, we present a small-size single-photon oceanic lidar having underwater detection capabilities. To realize the long-range detection, we applied a single-photon detector to enhance the sensitivity of the lidar. A low-power laser with a pulse energy of micropulse and a small-aperture coupler with an aperture of 12 mm was applied. To realize high spatial resolution detection of underwater targets, we employed a picosecond pulse laser and a high-precision time-to-digital converter (TDC). This picosecond laser has a high repetition rate, which enables the capability of high update-rate detection. In this letter, we demonstrate single-photon underwater detection at ranges up to 105 m with 1-s temporal resolution. Furthermore, dynamic detection capability is demonstrated by monitoring underwater bubbles 26 m away from the lidar at a frequency of 100 Hz.

The schematic of the single-photon lidar system setup is shown in Fig. 1. The system employs a compact fiber-based laser operating at 532 nm. The beam divergence of the laser is 0.5 mrad. A fiber-connected configuration is specially designed for the miniaturized and robust structure. The backscattered signal from the water is coupled in a 105-μm multimode fiber (MMF) by a collimator with 27.5-mm focal length, which corresponds to the field of view (FOV) of ~3.8 mrad. This narrow receiving FOV in our lidar system offered significant background noise suppression. The distance between the transmitted laser and the received coupler is ~15 mm. A 532-nm filter with bandwidth of 0.2 nm is used to further block the background noise. Finally, a compact free-running silicon single-photon avalanche diode (SPAD) is adopted. It has an efficiency of ~52% with 100 dark counts per second (cps). Also, the time jitter of the detector was measured at ~300 ps.

As to the electronic module, a homemade function generator (FG) based on field-programmable gate array (FPGA) provides a precise control signal for laser, SPAD detector, TDC, and scanning mirror. A high-precision TDC with 13-ps resolution is adopted to record the time of pulse emission and photon detection. A summary of the system parameters is listed in Table I.

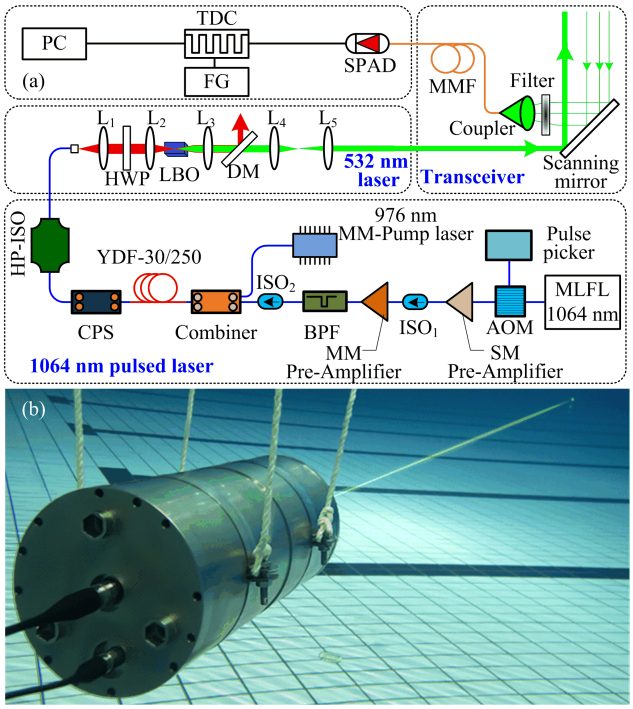

Fig. 1. (a) Schematic of the single-photon underwater lidar. MLFL: mode-locked fiber laser; AOM: acoustic-optical modulator; ISO: isolator; SM: single mode; MM: multimode; BPF: bandpass filter; YDF: Yb-doped fiber; CPS: cladding power stripper; HP-ISO: high-power optical isolator; HWP: half-wave plate; LBO: lithium borate; DM: dichroic mirror; MMF: MM fiber; SPAD: single-photon avalanche diode; TDC: time-to-digital converter; FG: function generator; and PC: personal computer. (b) Photograph of the underwater lidar.

TABLE I
Key Parameters of the Underwater Single-Photon Lidar

Parameters	Value
Pulsed Laser	
Wavelength (nm)	532
Pulse duration (ps)	501
Pulse energy (μJ)	1
Pulse repetition rate (MHz)	1
Beam divergence (mrad)	0.5
Coupler	
Aperture (mm)	12
Focal length (mm)	27.5
Mode-field diameter (μm)	105
FOV (mrad)	3.8
Silicon APD	
Detection efficiency at 532 (%)	52
Dark count (cps)	100

A photograph of the underwater lidar system is shown in Fig. 1(b). The lidar system is made of titanium alloy with high-pressure resistance properties so that the lidar can operate

underwater up to 2 km. The optical window of the lidar is made of sapphire lens, which can maintain ≥96% transmission under high pressure. The cylindrical lidar has a diameter of 20 cm and a length of 40 cm. The average power consumption of the lidar is less than 100 W. To enhance the spatial resolution and temporal resolution, a watt-level, narrow-linewidth, all-polarization-maintaining (PM) green laser with a repetition rate of 1 MHz is employed. Our picosecond green laser consists of a 1064-nm picosecond seed laser, a pulse picker, a master oscillator power amplifier (MOPA), and a lithium borate (LBO)-based frequency doubling unit.

The picosecond seed laser is generated by a passively mode-locked fiber laser (MLFL) with a 1063.92-nm central wavelength. The seed laser is then connected to a pulse picker, i.e., a synchronization-triggered acoustic-optical modulator (AOM), which acts as a frequency demultiplier to reduce the repetition rate to 1 MHz. The 1064-nm picosecond laser at a 1-MHz repetition rate is further amplified by the MOPA. The MOPA is constructed by a single-mode (SM) Yb-doped fiber (YDF) preamplifier, a multimode (MM) YDF preamplifier, and a main amplifier. The SM preamplifier uses a piece of single-clad PM YDF pumped by a 976-nm SM laser diode (LD). Then, the MM preamplifier comprises a 10-μm-core double-clad PM YDF pumped with an MM 976 nm LD using a fiber combiner. To prevent the amplified spontaneous emission (ASE), a 0.5-nm bandpass filter (BPF) at 1064 nm is used in the output port of the MM preamplifier. Finally, the main power amplifier is realized by a large-core double-clad PM YDF (30-μm core, NA = 0.08; 250-μm inner cladding, NA = 0.46). A cladding power stripper (CPS) is adopted to remove the residual pump power, and a high-power optical isolator (HP-ISO) is used to protect the amplifier from possible damage caused by backscattered light. Finally, up to 3.5 W of average power is achieved with a pulse duration of 501 ps and a repetition rate of 1 MHz.

Subsequently, the frequency doubling from 1064 to 532 nm is performed. A plane convex lens (L1) is employed to collimate the 1064-nm amplified laser from the ferrule connector/angled physical contact (FC/APC) connector. A half-wave plate (HWP) is used to adjust the linear polarization direction of the 1064-nm laser to meet the phase-matching condition of LBO crystal. The 1064-nm picosecond pulses are then focused onto the LBO crystal in a heated oven. After the LBO crystal, a plane convex lens (L3) is used to collimate the 532-nm green light, and a 45° harmonic separator [i.e., 532-/1064-nm dichroic mirror (DM)] is used to remove the residual 1064-nm laser. A pure green light at 531.96 nm is obtained. The average output power reaches 1 W. As shown in Fig. 2, the laser linewidth maintains a narrow one of 0.04 nm (full-width at half-maximum), and the pulsewidth is 501 ps. The pulse energy and peak power of the narrow-linewidth picosecond green laser are 1 μJ and 2 kW, respectively, which could be very favorable to long-range, high-resolution oceanic lidar.

III. Experiment

Here, we present a field experiment to demonstrate underwater performance, including long-distance and high-speed

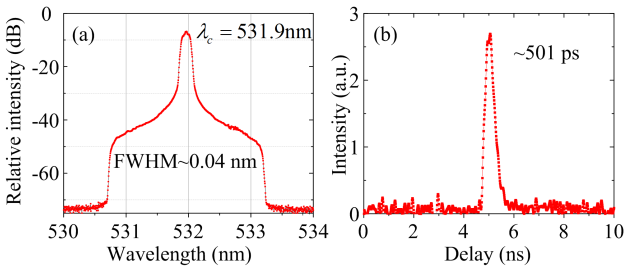

Fig. 2. Performance of the watt-level, narrow-linewidth all-PM picosecond green laser system. (a) Output optical spectrum. (b) Laser pulse.

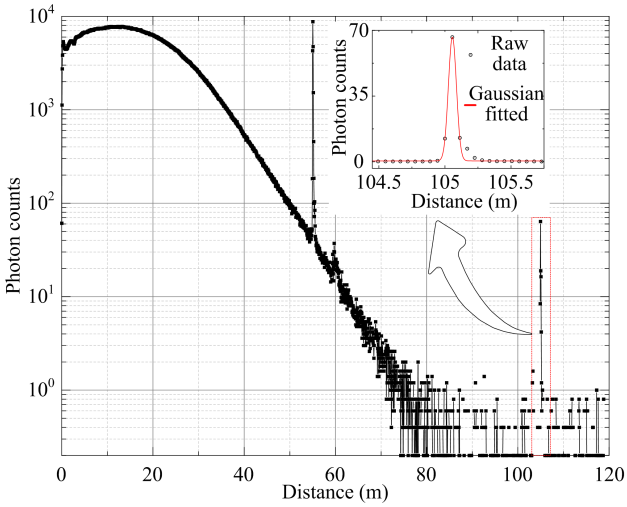

Fig. 3. Raw signals of the single-photon lidar.

underwater detection capabilities. A field experiment was carried out in a swimming pool at the Xiang'an campus of Xiamen University (2437′N, 11818′E). The size of the pool is 50 × 25 × 2 m.

To demonstrate that our lidar can detect objects at distances greater than 50 m, a 300 × 300 mm mirror with a high reflection rate of >95% at 532 nm was placed on the wall of the pool to reflect the laser. The raw profile with 1-s temporal resolution and 0.5-ns sample ratio is plotted in Fig. 3, where the detection distance of waterbody backscattered signal is more than 70 m at the signal-to-noise ratio (SNR) ≥ 2, and the backscattered signal from the wall at a distance of ∼105 m at the SNR ≥ 50 also detected. Due to the proximity of the transmitter and receiver telescopes and the multiple scattering signals contained in the backscattered signal caused by the strong forward scattering of the water, the lidar signal can be measured from 0 m. As the laser beam and the received FOV tends to overlap, the intensity of the backscattered signal first increases and then decreases with distance. Once the geometric overlap reaches 100%, the backscattered signal decays exponentially from ∼25 m. The first peak of the profile at ∼55 m is due to the reflection of the high reflection mirror. The peak immediately following the peak at 55 m, at around 60 m, is caused by the afterpulsing of the SPAD and can be corrected using an appropriate algorithm [24].

To validate the time jitter characteristics of the lidar system, the raw signal of the target at ∼105 m was extracted and fit using a Gaussian function, as shown in the small insert in

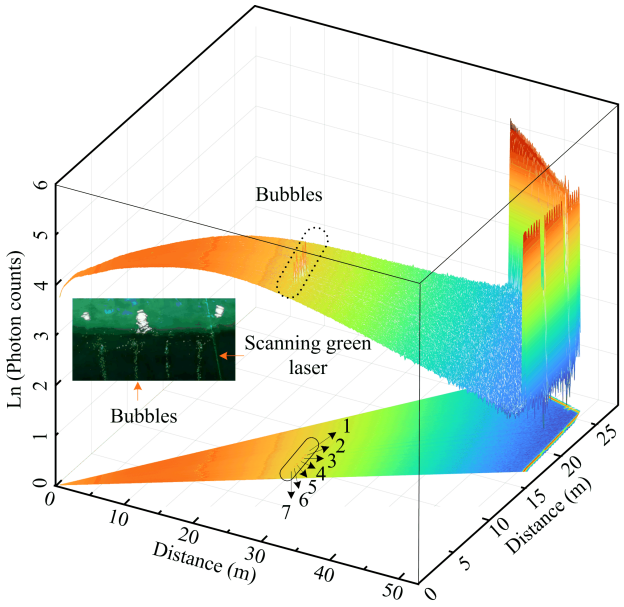

Fig. 4. Scanning pattern to locate bubbles in the swimming pool.

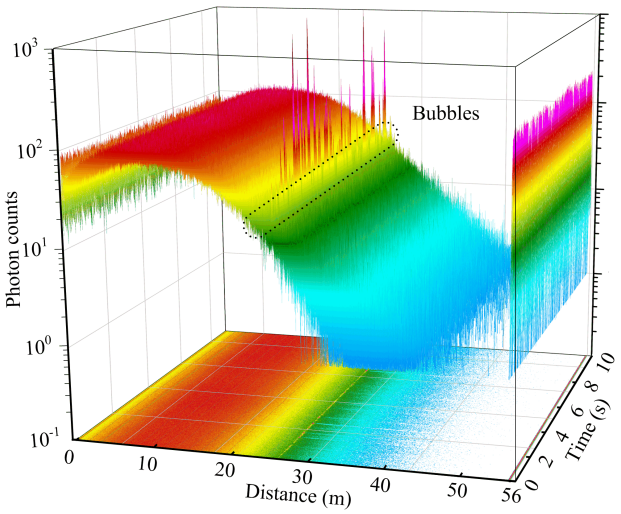

Fig. 5. Sensing the bubbles with the refresh rate of 100 Hz.

Fig. 3. The width of the fit Gaussian function is ∼0.6 ns, which is the total time jitter of the system, determined by the laser pulsewidth, pulse jitter, timing jitter of the SPAD, and the sample rate of the TDC. By using the lidar to measure small displacements of a hard target, we have validated that the lidar's depth resolution along the beam direction is approximately 5.6 cm.

Using an absorption and attenuation meter ac-9 (WET Labs, Inc.), the absorption coefficient (a) and the beam attenuation coefficient (c) at 532 nm were simultaneously measured. The backscattering coefficient b_b at 532 nm was calculated by interpolating b_b at 488 and 550 nm, which were measured by HOBI Labs HS6P. The measured a, b_b, and c at 532 nm were 0.044, 0.0035, and 0.07 m^{-1}, respectively. The traditional method for estimating the lidar attenuation coefficient (K_{lidar}) from 30 to 50 m resulted in an attenuation coefficient K_{lidar} of ∼0.064 m^{-1}, which is consistent with the conclusion that K_{lidar} is approximately equal to c in the case of narrow receiver FOV [25]. With a diffuse attenuation coefficient model, where $K_d = m_0 a + m_1[1 - m_3 \exp(-m_3 b_b)]$ and (m_0, m_1, m_2, m_3) are model parameters [26], the estimated K_d is ∼0.052 m^{-1}. Based on the measured results shown in Fig. 3, the detection range can reach ∼3.6/K_d for this water body and up to 5.5/K_d for hard target.

To demonstrate the robustness and flexibility of the lidar system, the lidar was switched to the scanning mode. The personal computer (PC)-controlled scanning mirror was used to scan the beam with a scanning step of 1.05 mrad, a scanning angle of 18° (0.314 rad), and scanning from left to right. As shown in Fig. 4, the lidar can accurately locate seven bubble points generated by the bubble generator, with a bubble diameter of approximately 1 mm. During the scanning process, the angular deviation caused by the refraction of the laser through different media (mirrors and water) was corrected using the Fresnel formula. As can be seen from Fig. 4, after correction, the reconstructed walls of the swimming pool are straight.

The high update-rate detection capability of our lidar makes it possible to capture underwater moving objects. In the experiment, the fixed pointed lidar that transmitted a laser beam through a bubble at approximately 26 m away. The temporal resolution of the backscattered profile was adjusted to 0.01 s (100-Hz update rate). As shown in Fig. 5, the number of bubbles passing through the laser beam per unit of time can be calculated, which is estimated as ∼10 bubbles per second.

IV. Conclusion

In conclusion, we developed a compact all-fiber single-photon underwater lidar with high spatial–temporal resolution based on a fiber-based picosecond laser and a single-photon detector. The field experiment demonstrated that this lidar has long-range detection and high update-rate detection capabilities in clean water. The results suggest that single-photon lidar can be a powerful tool not only for mapping the spatial extent of thin scattering layers and linking their occurrence to larger scale physical processes but also for tracking their evolution over time and guiding the ship-based sampling needed to understand their composition, dynamics, and impacts. In the future, we plan to focus on improving the performance of our lidar system, such as daytime operation, depolarization, and fluorescence detection. We will also operate this lidar in different conditions, including in coastal water and the ocean, to further verify its performance. Since the interference from the sea–air interface and atmospheric backscattered signals can be avoided, underwater lidar signals can potentially be used as true values to calibrate oceanic lidars that operated above the water. In particular, this lidar will be deployed in AUVs, which will provide us with a new view to better understand the ocean biogeochemical cycle.

References

[1] M. J. Behrenfeld et al., "Global satellite-observed daily vertical migrations of ocean animals," *Nature*, vol. 576, no. 7786, pp. 257–261, Dec. 2019.

[2] C. A. Hostetler, M. J. Behrenfeld, Y. Hu, J. W. Hair, and J. A. Schulien, "Spaceborne LiDAR in the study of marine systems," *Annu. Rev. Mar. Sci.*, vol. 10, no. 1, pp. 121–147, Jan. 2018.

[3] S. Zhang and P. Chen, "Subsurface phytoplankton vertical structure from LiDAR observation during SCS summer monsoon onset," *Opt. Exp.*, vol. 30, no. 11, pp. 17665–17679, 2022.

[4] A. Rudolf and T. Walther, "Laboratory demonstration of a Brillouin LiDAR to remotely measure temperature profiles of the ocean," *Opt. Eng.*, vol. 53, no. 5, Jan. 2014, Art. no. 051407.

[5] Y. Wang et al., "Brillouin scattering spectrum for liquid detection and applications in oceanography," *Opto-Electron. Adv.*, vol. 6, Jan. 2022, Art. no. 220016.

[6] J. H. Churnside, "LiDAR signature from bubbles in the sea," *Opt. Exp.*, vol. 18, no. 8, pp. 8294–8299, 2010.

[7] J. H. Churnside and L. A. Ostrovsky, "LiDAR observation of a strongly nonlinear internal wave train in the Gulf of Alaska," *Int. J. Remote Sens.*, vol. 26, no. 1, pp. 167–177, Jan. 2005.

[8] J. H. Churnside and J. A. Shaw, "LiDAR remote sensing of the aquatic environment," *Appl. Opt.*, vol. 59, no. 10, pp. 92–99, 2020.

[9] D. McLeod, J. Jacobson, M. Hardy, and C. Embry, "Autonomous inspection using an underwater 3D LiDAR," in *Proc. OCEANS*, 2013, pp. 1–8.

[10] Q. Liu et al., "Shipborne variable-FOV, dual-wavelength, polarized ocean LiDAR: Design and measurements in the Western Pacific," *Opt. Exp.*, vol. 30, no. 6, pp. 8927–8948, 2022.

[11] P. Chen et al., "Vertical distribution of subsurface phytoplankton layer in South China sea using airborne LiDAR," *Remote Sens. Environ.*, vol. 263, Sep. 2021, Art. no. 112567.

[12] X. Lu, Y. Hu, C. Trepte, S. Zeng, and J. H. Churnside, "Ocean subsurface studies with the CALIPSO spaceborne LiDAR," *J. Geophys. Res., Oceans*, vol. 119, no. 7, pp. 4305–4317, Jul. 2014.

[13] X. Lu et al., "New ocean subsurface optical properties from space LiDARs: CALIOP/CALIPSO and ATLAS/ICESat-2," *Earth Space Sci.*, vol. 8, no. 10, 2021, Art. no. e2021EA001839.

[14] G. Mandlburger, M. Pfennigbauer, R. Schwarz, S. Flöry, and L. Nussbaumer, "Concept and performance evaluation of a novel UAV-borne topo-bathymetric LiDAR sensor," *Remote Sens.*, vol. 12, no. 6, p. 986, Mar. 2020.

[15] S. E. Mitchell and J. P. Thayer, "Ranging through shallow semitransparent media with polarization LiDAR," *J. Atmos. Ocean. Technol.*, vol. 31, no. 3, pp. 681–697, Mar. 2014.

[16] D. Ventura, "Coastal zone mapping with the world's first airborne multibeam bathymetric LiDAR mapping system," in *Hydrographische Nachrichten 115* (DeutscheHydrographische Gesellschaft e.V. S.), 2020, pp. 48–53.

[17] B. L. Collister, R. C. Zimmerman, C. I. Sukenik, V. J. Hill, and W. M. Balch, "Remote sensing of optical characteristics and particle distributions of the upper ocean using shipboard LiDAR," *Remote Sens. Environ.*, vol. 215, pp. 85–96, Sep. 2018.

[18] K. Li et al., "A dual-wavelength ocean LiDAR for vertical profiling of oceanic backscatter and attenuation," *Remote Sens.*, vol. 12, no. 17, p. 2844, Sep. 2020.

[19] J. Ma et al., "Compact dual-wavelength blue-green laser for airborne ocean detection LiDAR," *Appl. Opt.*, vol. 59, no. 10, p. 87, 2020.

[20] J. Degnan, "Scanning, multibeam, single photon LiDARs for rapid, large scale, high resolution, topographic and bathymetric mapping," *Remote Sens.*, vol. 8, no. 11, p. 958, Nov. 2016.

[21] M. Shangguan et al., "All-fiber upconversion high spectral resolution wind LiDAR using a Fabry–Perot interferometer," *Opt. Exp.*, vol. 24, no. 17, pp. 19322–19336, 2016.

[22] M. Shangguan et al., "Dual-frequency Doppler LiDAR for wind detection with a superconducting nanowire single-photon detector," *Opt. Lett.*, vol. 42, no. 18, pp. 3541–3544, 2017.

[23] X. Shen, W. Kong, P. Chen, T. Chen, G. Huang, and R. Shu, "A shipborne photon-counting LiDAR for depth-resolved ocean observation," *Remote Sens.*, vol. 14, no. 14, p. 3351, Jul. 2022.

[24] C. Yu, M. Shangguan, H. Xia, J. Zhang, X. Dou, and J.-W. Pan, "Fully integrated free-running InGaAs/InP single-photon detector for accurate LiDAR applications," *Opt. Exp.*, vol. 25, no. 13, pp. 14611–14620, 2017.

[25] H. R. Gordon, "Interpretation of airborne oceanic LiDAR: Effects of multiple scattering," *Appl. Opt.*, vol. 21, no. 16, pp. 2996–3001, Aug. 1982.

[26] Z.-P. Lee, "A model for the diffuse attenuation coefficient of downwelling irradiance," *J. Geophys. Res.*, vol. 110, no. 2, pp. 1–10, 2005.